Estimating the uncertainties of strain and damage analysis by X-ray diffraction in ion implanted MoO₃

D. R. Pereira[1,2*], S. Magalhães[2], C. Díaz-Guerra[3], M. Peres[2], J. G. Correia[4], J. G. Marques[4], A. G. Silva[5], E. Alves[2], S. Cardoso[1], P. P. Freitas[1,6], K. Lorenz[1,2**]

[1] Instituto de Engenharia de Sistemas e Computadores – Microsistemas e Nanotecnologias (INESC MN), Lisbon, Portugal

[2] IPFN, Instituto Superior Técnico, Universidade de Lisboa, Portugal

[3] Departamento de Física de Materiales, Facultad de Ciencias Físicas, Universidad Complutense de Madrid, Madrid, Spain

[4] Centro de Ciências e Tecnologias Nucleares, Departamento de Engenharia e Ciências Nucleares, Instituto Superior Técnico (IST), Universidade de Lisboa, Portugal

[5] Cefitec, Departamento de Física, Faculdade de Ciências e Tecnologia, Universidade Nova de Lisboa, Campus da Caparica, Portugal

[6] INL - International Iberian Nanotechnology Laboratory, Braga, Portugal

[*]Corresponding Author: danielapereira@ctn.tecnico.ulisboa.pt

[**]Corresponding Author: lorenz@ctn.tecnico.ulisboa.pt

Abstract

Ion implantation of oxygen in MoO₃ lamellar crystals allows tuning their electrical conductivity by defect formation. X-ray diffraction (XRD) is a particularly sensitive technique to study such defects that cause changes in the lattice parameters and crystal quality. In this work, dynamical theory was applied to fit XRD patterns to obtain the strain and static Debye-Waller (DW) factor distributions as a function of depth. A two-step method was tested to estimate the uncertainties of these parameters within a certain region of interest. The limitations of the XRD characterization to study regions with low values of static DW factor are discussed.

Keywords: Molybdenum Oxide, Ion Implantation, X-ray Diffraction (XRD), strain, static Debye-Waller (DW) factor

1. Introduction

Molybdenum oxide (MoO_3) is a wide band gap semiconductor crystallizing in the orthorhombic phase, which is thermodynamically stable at room temperature (α-MoO_3).[1] An interesting feature of α-MoO_3 is the possibility to tune the electrical properties of this material by creating oxygen vacancies. For example, depending on the MoO_x stoichiometry, samples show semiconducting behavior for MoO_{3-x} ($2 < x \leq 3$) and metallic behavior for MoO_2.[2,3]

The possibility of tuning the electrical properties of MoO_3 lamellar crystals using 170 keV oxygen ion implantation to create defects was explored in ref. [4]. Based on I-V measurements of these implanted crystals, a significant and reproducible increase of conductivity was reported after implantation to fluences above 1×10^{15} cm^{-2}. Furthermore, a detailed study of the evolution of defects induced by implantation was realized, based on the evolution of the strain and damage (static Debye-Waller (DW) factor) profiles obtained by simulation of X-ray diffraction (XRD) curves with the RaDMaX (Radiation Damage in Materials analyzed with X-ray diffraction) software.[4] XRD has been used in many crystalline materials to investigate the strain introduced by implantation defects. [5–15] However, the estimation of the uncertainties associated with the strain and damage profiles is challenging since the fit results strongly depend on the considered fitting model. Therefore, simple statistical methods evaluating the goodness of fit may not be meaningful. Indeed, distinct combinations of strain and damage profiles may give similarly good fits.

In this paper, we present a two-step method to estimate and validate the uncertainties associated with the strain and damage profiles obtained from the fits of the XRD measurements. As an application example, the uncertainties associated with the strain and static DW factor values will be analyzed within the depth region of maximum nuclear energy deposition, for a fluence range from 5×10^{12} cm^{-2} to 1×10^{17} cm^{-2}.

2. Experimental Details

α-MoO_3 lamellar crystals, with typical thicknesses of few micrometers and lateral dimensions of about 2×5mm^2, were grown by an evaporation-solidification method, described in detail in refs. [4,16,17]. Briefly, this method consists of placing a compacted Mo powder disc at the center of a horizontal tube furnace, where the temperature of 750ºC and an air flow of 2l/min are set for 10h. Under these conditions, the Mo is oxidized in contact with the air and is transported to the tube extremities, where MoO_3 deposits due to the existing temperature gradient. The crystals were then fixed on Si or glass substrates using Kapton tape or silver ink, so that they can be implanted and characterized.

The ion implantation process was done at room temperature with 170 keV oxygen ions and for a fluence range from 1×10^{12} cm^{-2} to 1×10^{17} cm^{-2}.[4] The expected defects and implanted oxygen ions profiles obtained by the SRIM 2013 (Stopping and Ranges of Ions in Matter) Monte Carlo simulations [18] are shown in figure 1.

In order to evaluate the structural changes, XRD 2θ−ω measurements of the 060 reflection of MoO$_3$ were performed on a Bruker D8 Discover high resolution diffractometer. The primary beam optics is constituted of a Göbel mirror, a 0.2 mm collimation slit and a 2-bounce Ge (220) monochromator to select the K_{α_1} X-ray radiation of copper (λ = 1.5406Å). In the secondary path, a 0.1 mm slit was placed in front of the scintillation detector. By fitting the XRD curves using the RaDMaX software [19], the strain and static DW factor profiles were obtained. The static DW factor is used as a measure of the damage in the lattice and it is given by $\int du_z . p(\delta u_z)\exp(iQ\delta u_z)$, where $Q = 4\pi sin(\theta)/\lambda$ is the scattering vector length and, $p(\delta u_z)$ is the probability distribution function of the random atomic displacement at depth z (δu_z). [20,21] This factor has an impact on the simulated diffraction intensity, and can take a minimum value of 0 for fully damaged crystals (amorphized or heavily disordered), and a maximum value of 1 for a perfect crystal. [20,22]
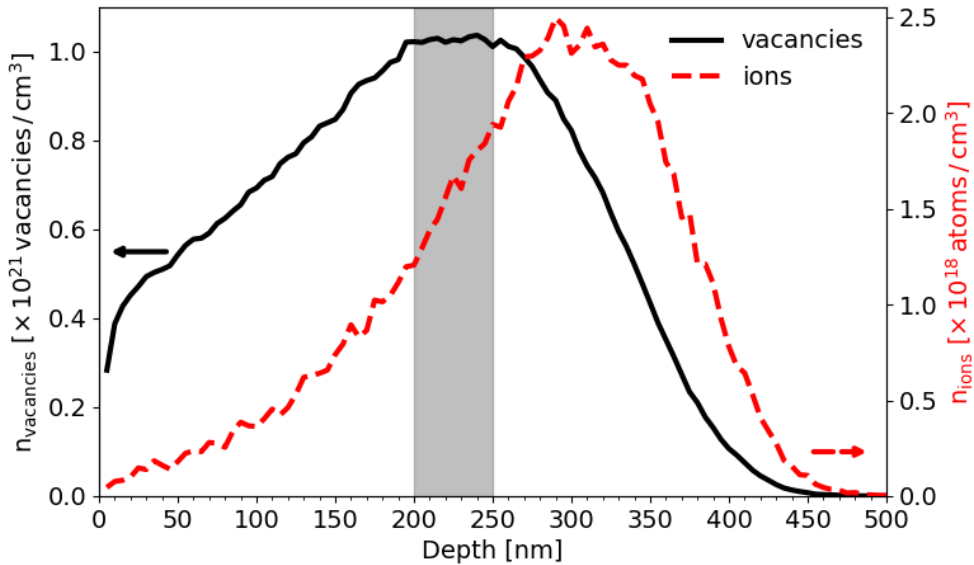

Figure 1 – Depth-profiles of the concentration of oxygen vacancies (solid black line) and implanted oxygen ions (dashed red line) obtained from SRIM simulations for the fluence of 5×10^{13} cm^{-2}. The grey area represents the region of interest (ROI) where the concentration of defects is expected to be maximum.

3. Results and Discussion

Figure 2 shows the evolution of the average strain and static DW factor as a function of the oxygen fluence, in the region of interest (ROI) represented in figure 1 by the grey area. This ROI corresponds to the depth at which the energy deposition by nuclear collisions, and hence the

concentration of primary defects, is maximum. Analyzing figure 2, it is possible to observe a moderate increase of the average strain, accompanied by a decrease of the average static DW factor for fluences below 7.5×10^{13} cm^{-2}, which was attributed to the formation of point defects [4]. When the fluence increases, a more significant increase of the average strain is observed, followed by a saturation at values of about 2.5%. On the other hand, the average of the static DW factor continues to decrease with increasing fluence, reaching values close to zero for the fluences above 1×10^{15} cm^{-2}. Similar strain and damage accumulation curves are observed in many ion implanted materials such as III-nitrides, III-V arsenides, cubic zirconia, and oxide materials (for example MgO, ZnO and UO_2)[5,6,8–12,14,23], where the strain saturation was attributed to the morphological alteration of the defect structures (from simple point defects to more complex defects), promoted by the high mobility of point defects during the implantation process. Figure 2 also shows the estimated uncertainties associated with the average strain and static DW factor values for each fluence, obtained by the method described in detail below.
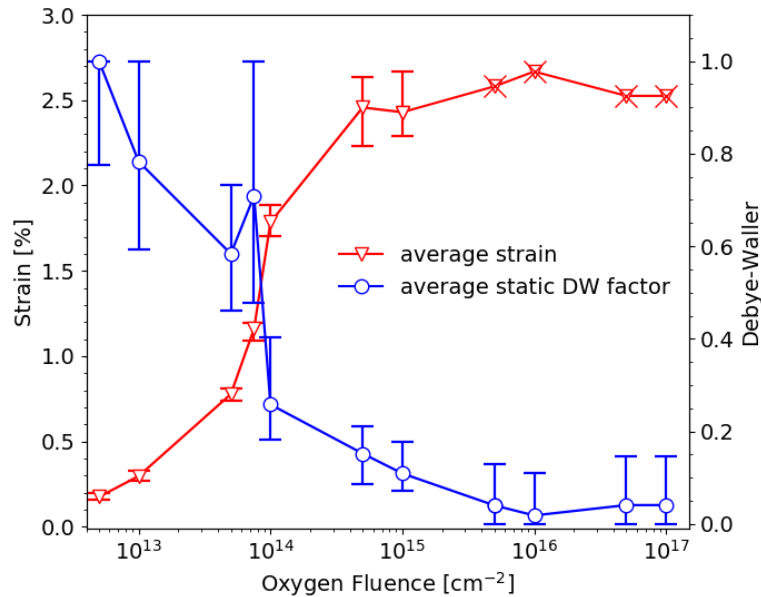
Figure 2 - Evolution of the average strain and static DW factor in the region of interest (ROI) marked in figure 1 and, respective uncertainties. Symbols that correspond to the average values with very high experimental uncertainties are crossed out (see text for a detailed discussion).

The method used to estimate the uncertainties shown in figure 2 is composed of two steps, both implemented using the RaDMaX software [19]. The first step consists in modifying slightly the strain and damage profiles in the whole implanted region (so as not to change the shape of the profiles) until the fit obtained was no longer acceptable. For quantification purposes, we define the increase of the root-mean-square error (Δrms) given by equation (1):

$$\Delta\text{rms} = \frac{\text{rms}(\exp, \text{sim}) - \text{rms}(\exp, \text{fit})}{\text{rms}(\exp, \text{fit})} \times 100\% \qquad (1)$$

where, the root-mean-square error (rms) calculated from the experimental diffractogram and the original fit – rms(exp, fit) – and, that from the experimental diffractogram and the simulations using the modified strain/static DW factor profiles – rms (exp, sim) – are given by equation (2):

$$\text{rms (exp, fit/sim)} = \sqrt{\frac{\sum_{i=1}^{N} \left[log\left(I_i^{exp}\right) - log\left(I_i^{fit/sim}\right) \right]^2}{N}} \tag{2}$$

with N being the number of data points and, I_i^{exp} and $I_i^{fit/sim}$ the normalized intensities of the experimental and calculated XRD curves, respectively. Note that, the rms error is widely used by XRD curve fitting programs to optimize the strain and damage profiles.[24–26]

An example of this analysis is presented in figure 3 for the fluence of 5×10^{13} cm^{-2}. Observing the experimental curve in figure 3.(a), it is clear that after implantation a second peak at $2\theta \approx 38.73°$ is formed slightly shifted to lower 2θ angles from the main Bragg peak at ~39.01° (corresponding to the unimplanted deep regions of the sample). This new peak reveals an expansion of the *b* lattice parameter within the implanted layer. The experimental XRD curve can be well fitted assuming the strain and static DW factor profiles shown in figures 3.(b) and 3.(c) (black lines), respectively. The red lines in figure 3 represent the best fit of the experimental diffractogram whereas the blue and orange lines represent the simulations from the modified strain/static DW factor profiles. In figures 3.(a)-(c), a shift in the peak attributed to the implanted region from $2\theta \approx 38.73°$ towards lower angles is verified in the simulations, when the strain profile is changed in the direction of higher values (dashed blue line) and the static DW factor profile is kept constant. In contrast, when the strain profile is shifted to lower values (dotted orange line), maintaining the same static DW factor profile, there is an opposite behavior in which the peak initially at $2\theta \approx 38.73°$ moves towards higher angles. If a similar procedure is applied to the static DW factor profile, a different effect is observed in the simulated diffractogram as shown in figures 3.(d)-(f). When the static DW factor values are increased in the entire damaged region (dashed blue line), an increase in the peak intensity ($2\theta \approx 38.73°$) is observed. Contrary, if the static DW factor profile is moved to the lower values (dotted orange line), a decrease of peak intensity is verified. Indeed, such behavior is expected since a higher crystalline quality will lead to increased diffracted intensity, whereas an increase of material damage translates into a decrease in the intensity. In the first step (figure 3), the strain and static DW factor profiles were changed until the Δrms value increases to about 80%, considering the region defined by the black double arrow at the bottom of figures 3.(a) and 3.(d). This threshold value of Δrms = 80% was chosen to yield significant differences between the simulated and experimental diffractograms for the entire set of samples. Note that, as seen from equations (1) and (2), the Δrms value depends on the size of the analyzed

region and the order of magnitude of the intensity for each 2θ value, which can require different thresholds for Δrms, depending on the considered region and material in study. From the curves in figures 3.(b) and 3.(f), the average strain and static DW factor values in a certain region of the implanted layer can be determined and their uncertainties estimated by calculating the respective average values in the modified profiles. For the ROI, marked by the grey shaded area in figure 3, corresponding to the region of maximum nuclear energy deposition, the obtained uncertainties are shown in figure 2.
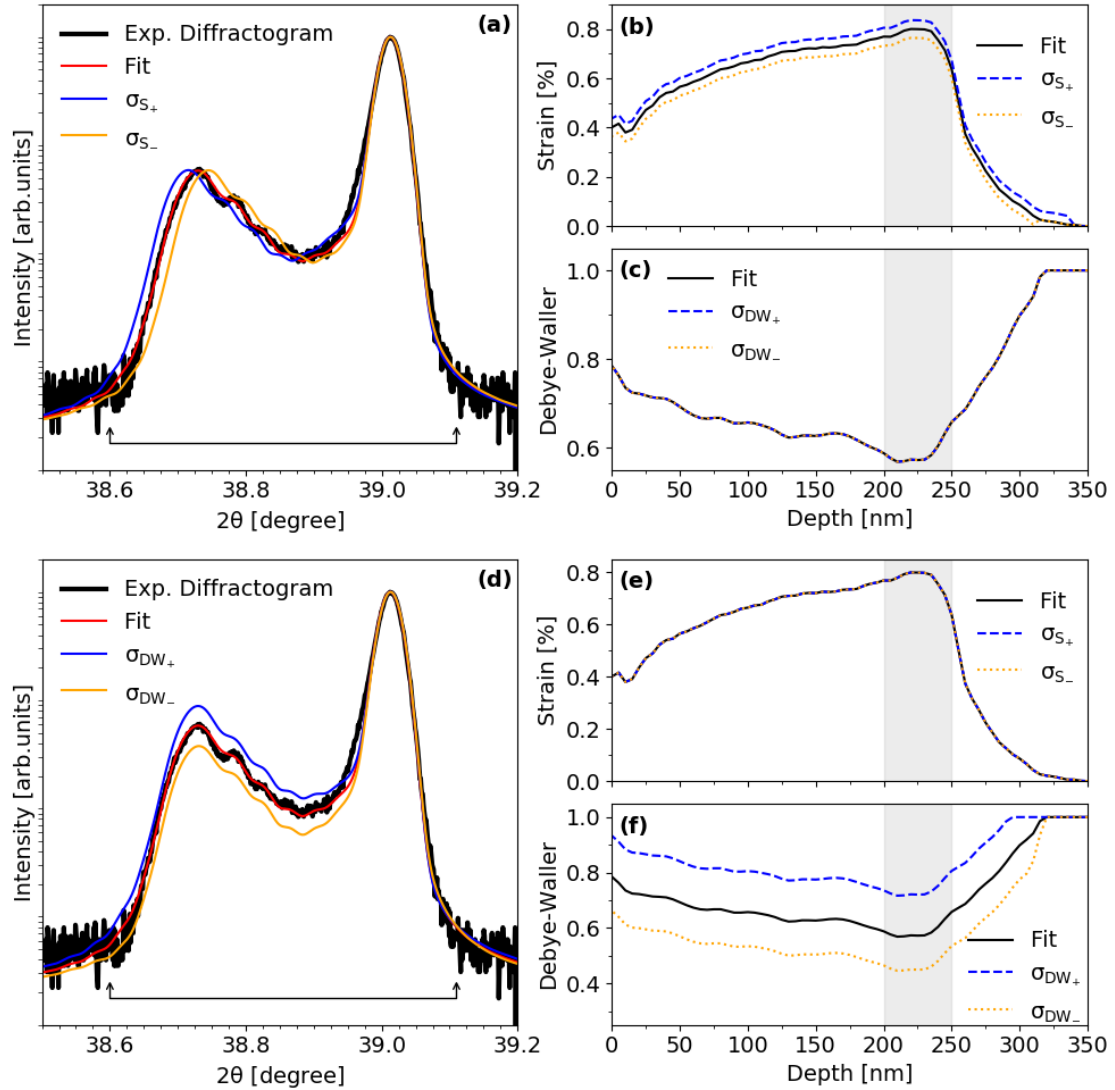
Figure 3 – Step 1: **(a)** Effect on the simulated XRD patterns of decreasing/increasing the **(b)** strain profile while maintaining a **(c)** fixed static DW factor profile. **(d)** Effect on the simulated XRD patterns of decreasing/increasing the **(f)** static DW factor profile while maintaining a **(e)** fixed strain profile. The Δrms value associated to the simulated XRD patterns is about 80% in the region delimited by the black double arrow at the bottom of **(a)** and **(d)**. The experimental diffractogram (black curves in **(a)** and **(d)**) and respective fit (solid red lines) are also shown. Experimental data corresponds to the fluence of 5×10^{13} cm^{-2}. The region of maximum nuclear energy deposition is indicated by the grey shaded area.

In the second step, the main goal is to evaluate in detail the influence of the ROI on the simulated diffractogram and use this information to validate (or discard) the uncertainties estimated in step one. For this, the strain and static DW factor values are changed only within the ROI, and the 2θ regions on the simulated diffractogram influenced by these changes are determined. For example, figures 4.(a)-(c) show that changing the strain in the ROI by the same factor as used in the first step (figure 3.(b)), changes only slightly the position of the maximum of the peak at $2\theta \approx 38.73º$. Instead, a widening and narrowing of the curve at $2\theta < 38.73º$ is verified when the strain values are increased and decreased inside the ROI, respectively. This behavior is expected, since the maximum of the diffraction peak has a strong contribution from less damaged regions with higher static DW factor values. For the case of the static DW factor - figures 4.(d)-(f) - an increase/decrease of the diffraction intensity at $2\theta \approx 38.73º$ and below is observed when the static DW factor values were increased/decreased within the ROI, to the same values represented in figure 3.(f). The differences between the fit and the simulated diffractograms, figures 4.(a) and 4.(d), show that the ROI mainly influences the simulated diffractograms in certain 2θ regions. The blue and orange double arrows at the bottom of the figures delimit the 2θ regions altered by the increase and decrease of the strain/static DW factor values inside the ROI. The different behaviors shown in figures 3 and 4, indicate that the methodology used in the first step can lead to unrealistic conclusions, since the main changes in the simulated diffractogram may not be due to the ROI. Note that, these discrepancies become more significant for high fluences where, within the ROI, the crystal is highly damaged. Thus, to validate the uncertainties obtained in the first step, it is crucial to confirm that the changes seen in the simulated diffractograms indeed reflect the changes in the properties within the ROI.
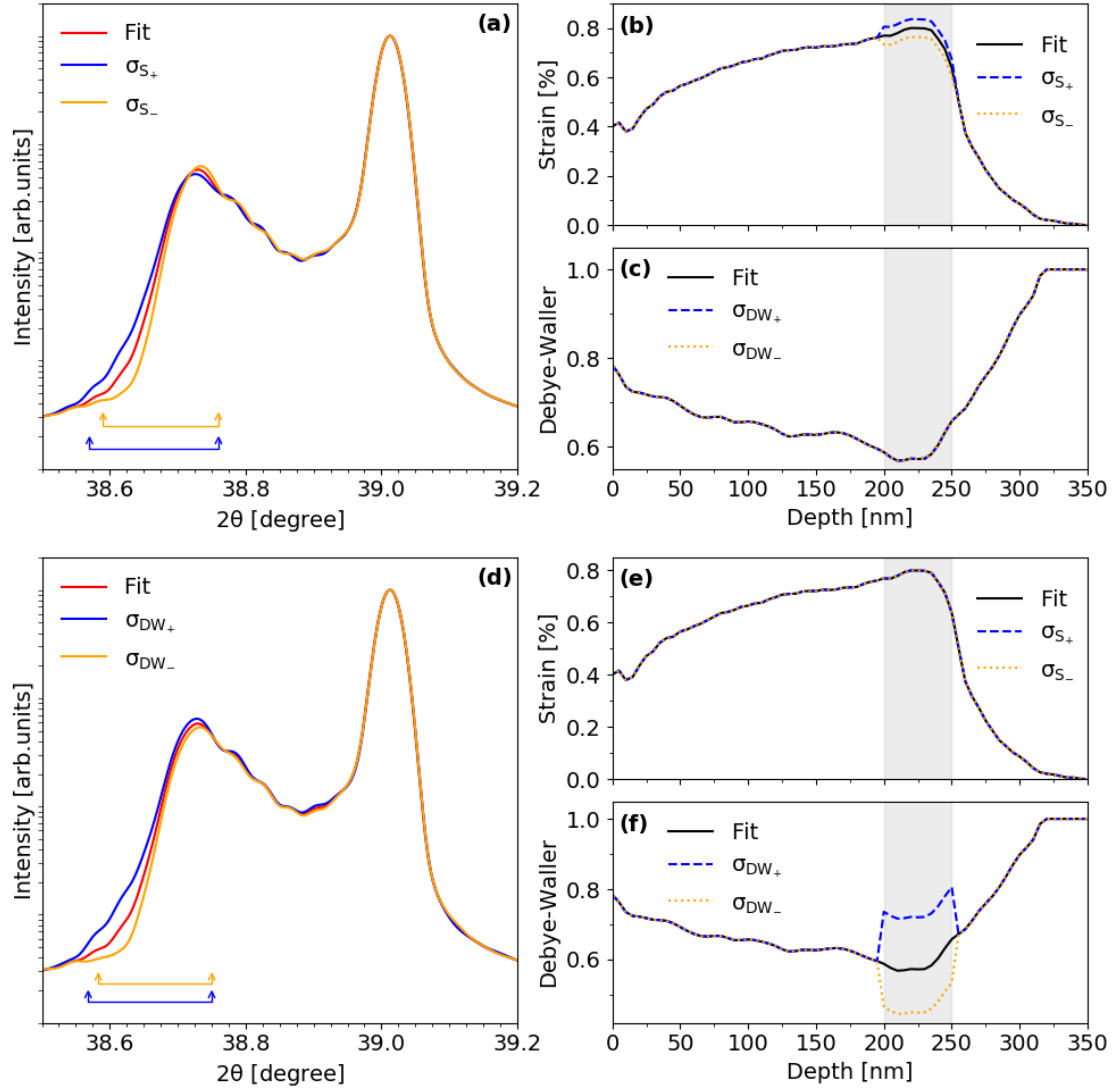
Figure 4 – Step 2: **(a)** Effect on the simulated XRD patterns of decreasing/increasing the **(b)** strain profile while maintaining a **(c)** fixed static DW factor profile, within the ROI. **(d)** Effect on the simulated XRD patterns of decreasing/increasing the **(f)** static DW factor profile while maintaining a **(e)** fixed strain profile, within the ROI. The strain and static DW factor values within the ROI were changed by the same factor as used in the first step (represented in figure 3). The best fit obtained by using the strain and static DW factor profiles given by the solid black lines is represented in **(a)** and **(b)** by the solid red lines. The region of maximum nuclear energy deposition is indicated by the grey shaded area. The orange and blue double arrows in **(a)** and **(d)** define the region of 2θ values influenced by the strain/ static DW factor values inside the ROI.

For the ROI considered here, the procedure used in step one clearly fails for the fluence of 5×10^{15} cm^{-2}, as shown in Figure 5. The red lines represent the best fit and, the black lines the respective strain and static DW factor profiles. Figure 5.(a) corresponds to the first step and shows the diffractograms (for which the Δrms is about 80%) obtained by simulations of the strain and damage profiles in figures 5.(b) and 5.(c), respectively. The second step is presented in figures 5.(d)-(f). Based on figure 5, it is possible to conclude that an increase/decrease of the strain values inside the ROI, keeping the respective static DW factor unchanged, causes only a slight modification in the simulated diffractogram for 2θ values delimited by the blue and orange double arrows at the bottom of figure 5.(d), a region where the signal-to-noise ratio is too low to draw any meaningful conclusion. This proves that the significant changes seen in the simulations of figure 5.(a) – corresponding to the step one - do not originate from the ROI and, therefore, the estimated uncertainties from this method have to be discarded. Such behavior is expected, since the static DW factor values are very low inside the ROI, with an average value of about 0.04 - figure 2. This means that the crystal is highly damaged and, consequently, the diffracted intensity arising from this region is extremely reduced. Indeed, when the static DW factor approaches zero, the strain can take a wide range of values without any visible change in the simulated diffractogram. In the present conditions, the static DW factor limit below which the strain is no longer well-defined was estimated to be about 0.06.[4] This value is very similar to that reported by A. Debelle et al. [14], where the diffracted intensity from cubic zirconia single-crystals was considered null, for regions where the static DW factor is below ~0.05. Thus, the uncertainties associated with the strain values in the ROI are very high, making these values meaningless. Note that in figures 5.(b) and 5.(e), an additional peak in the strain profile is seen at around 375 nm, as a possible consequence of the migration of point defects from regions of higher nuclear interaction to deeper regions in the sample (see ref.[4] for a detailed discussion).
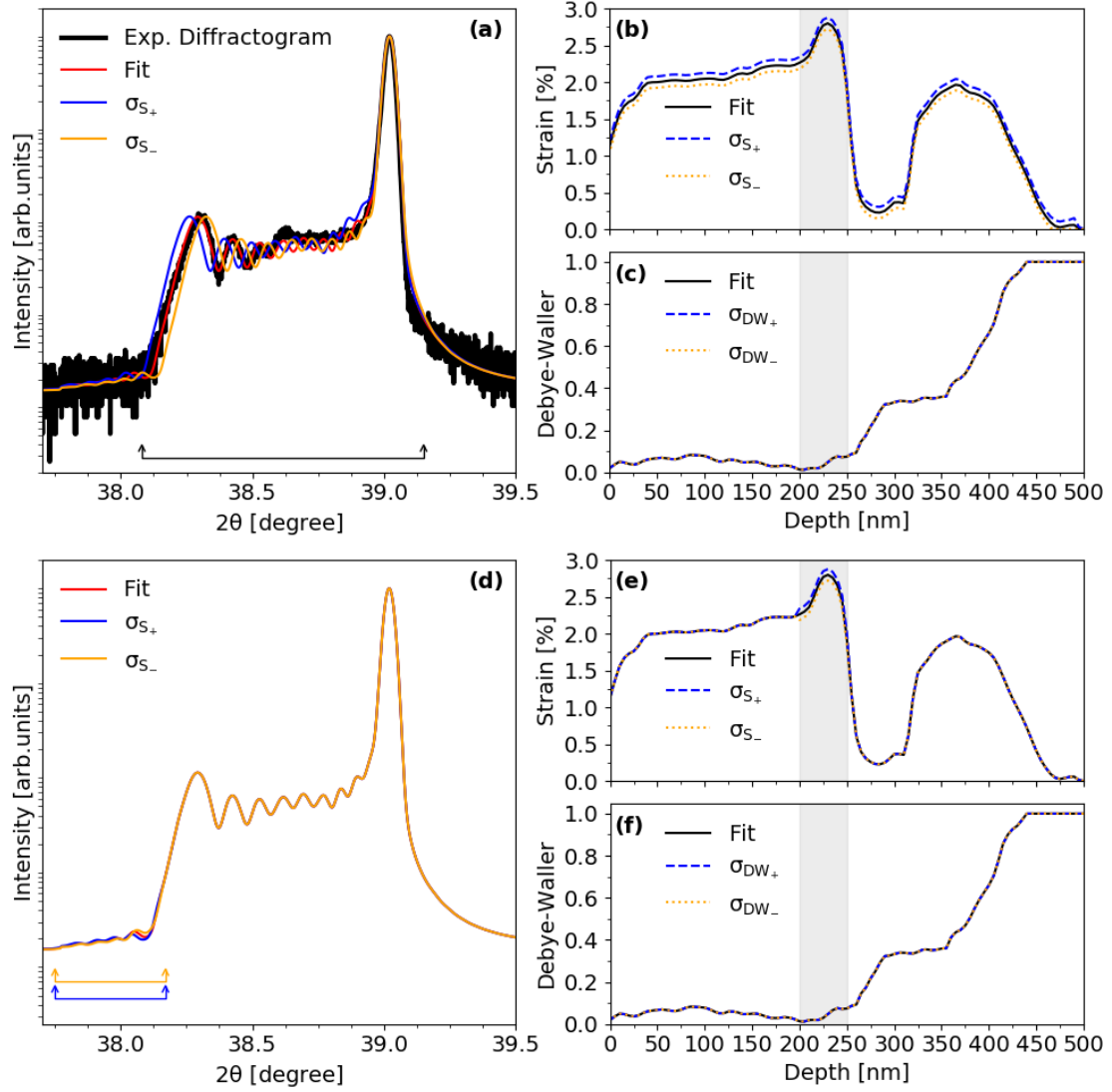
Figure 5 – (a-c) Step 1: (a) Effect on the simulated XRD patterns of decreasing/increasing the **(b)** strain profile while maintaining a **(c)** fixed static DW factor profile, so that Δrms $\approx$ 80%. **(d-f) Step 2: (d)** Effect on the simulated XRD patterns of decreasing/increasing the **(e)** strain profile while maintaining a **(f)** fixed static DW factor profile, within the ROI. Note that, the strain values inside the ROI have the same values in **(b)** and **(e)**. Experimental data corresponds to the fluence of 5×10^{15} cm^{-2}. The fit obtained by simulating the strain (solid black lines in **(b)** and **(e)**) and static DW factor profiles (solid black lines in **(c)** and **(f)**) is represented by the solid red line. The region of maximum nuclear energy deposition is indicated by the grey shaded area. The black double arrow in **(a)** represents the region where the Δrms was determined and, the orange and blue double arrows in **(d)** define the region of 2θ values influenced by the ROI.

Finally, it is possible to define a criterion which allows to validate (or discard) the uncertainty values estimated in step one. For this purpose, in the simulations obtained in step one, the increase in the root-mean-square error, Δrms$_{(ROI)}$, was calculated in the region of 2θ values influenced by the ROI (as defined in step two). Thus, it can be assumed that the first step provides a good estimation of the uncertainties when Δrms$_{(ROI)}$ is at least 80% (i.e. equal to or higher than the value obtained when considering the entire diffractogram). Figure 6 shows the evolution of Δrms$_{(ROI)}$

10

with the fluence, for the case of changing the strain profile. The $\Delta rms_{(ROI)}$ values are significantly greater than 80% for fluences below 1×10^{14} cm^{-2}, which means that the ROI has, locally, a high influence on the simulated diffractogram. Indeed, for low fluences, the average static DW factor values are higher than 0.25 inside the ROI (figure 2) and, therefore, the strain in that region will have a significant contribution to the obtained fit. When the fluence increases, the $\Delta rms_{(ROI)}$ values approach 80%, falling below for fluences above 1×10^{15} cm^{-2}. For these cases, our method cannot be validated, and the average strain values were crossed out in figure 2. In other words, the uncertainty becomes too large to determine any meaningful value for the average strain in the ROI. The first fluence for which this happens is 5×10^{15} cm^{-2} (shown in figure 5), where the average static DW factor value within the ROI is about 0.04. This value agrees well with the limit value of the static DW factor of 0.06 (limit below which no reliable strain values can be obtained) mentioned before and estimated in ref. [4]. In the case of static DW factor profiles, the $\Delta rms_{(ROI)}$ lies above 80% for all fluences (not shown) and, therefore, the respective estimated uncertainties within the ROI are validated.
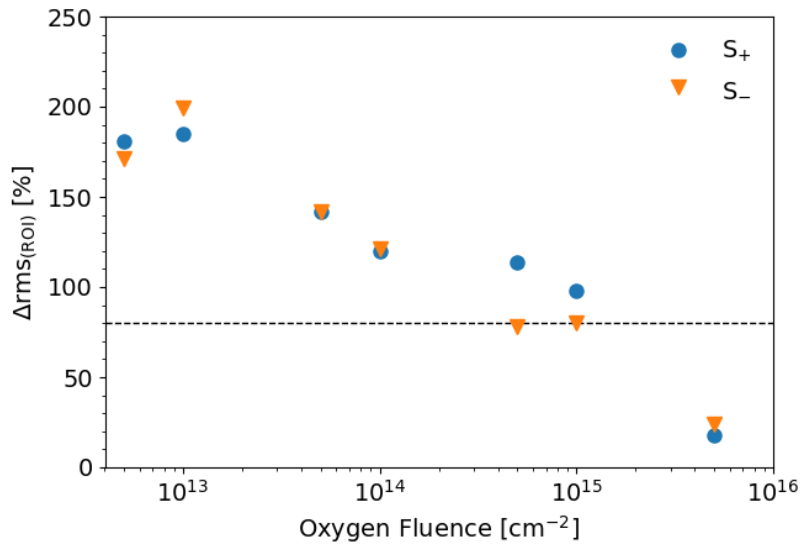
Figure 6 – Evolution, with increasing oxygen fluence, of the increase in the root-mean-square error - $\Delta rms_{(ROI)}$ - corresponding to the region of 2θ values influenced by the strain values inside the ROI. The blue dots (S$_+$) and orange triangles (S$_-$) represent the evolution of the $\Delta rms_{(ROI)}$ value caused by the increase and decrease of the strain values inside the ROI, respectively. The dashed black line represents the limit of 80% in the increase of the root-mean-square error.

4. Conclusion

Fitting XRD curves of ion implanted crystals using dynamical theory allows the extraction of strain and damage (static DW factor) profiles. However, the estimation of the associated uncertainties is not straightforward and, in fact, it is often omitted. In this paper, an empirical two-step method to evaluate these uncertainties is tested for a wide range of fluences. The depth region with the highest nuclear energy deposition (according to SRIM simulations), caused by 170 keV oxygen implantation in MoO_3, is used as a case study. After finding the best fit of the experimental diffractogram, the first step consists in changing the strain and static DW factor profiles in the entire implanted region, until the root-mean-square error increases by about 80%. Comparing the modified profiles with those of the best fit, the uncertainties associated with the average strain and static DW factor values inside a certain depth region (ROI) can be estimated. However, this method fails when the static DW factor within the ROI is very low and, consequently, the diffractogram is dominated by other less damaged depth regions of the sample. Therefore, a second step was implemented which allows validating the obtained uncertainties. In this step, the strain and static DW factor values are changed only within the ROI and the 2θ region influenced by these changes is determined. Then, using the simulations obtained in step one, the increase of the root-mean-square error in this 2θ region - $\Delta rms_{(ROI)}$ - can be calculated. The uncertainties of the average strain and static DW factor, obtained in the first step, are considered validated if the $\Delta rms_{(ROI)}$ value is higher than 80% (the limit established for considering the entire diffractogram). For this case, the static DW factor values inside the ROI are sufficiently high and, therefore, the respective strain values have an important contribution to the obtained diffractogram. On the other hand, a $\Delta rms_{(ROI)}$ value lower than 80% indicates that the static DW factor values within the ROI are too low. As the diffracted intensity from the highly damaged region is negligible, no reliable strain value can be determined. Finally, it is important to mention that the limit of 80% in the increase of the root-mean-square error is an empirical value and, therefore, may change depending on the depth region considered and material being studied.

References:

[1]   R.K. Sharma, G.B. Reddy, Controlled growth of vertically aligned MoO_3 nanoflakes by plasma assisted paste sublimation process, J. Appl. Phys. 114 (2013) 184310. doi:10.1063/1.4830278.

[2]   M. Dieterle, G. Mestl, Raman spectroscopy of molybdenum oxides. Part II. Resonance Raman spectroscopic characterization of the molybdenum oxides Mo_4O_{11} and MoO_2, Phys. Chem. Chem. Phys. 4 (2002) 822–826. doi:10.1039/b107046k.

[3]   D.O. Scanlon, G.W. Watson, D.J. Payne, G.R. Atkinson, R.G. Egdell, D.S.L. Law, Theoretical and Experimental Study of the Electronic Structures of MoO_3 and MoO_2, J. Phys. Chem. C. 114 (2010) 4636–4645. doi:10.1021/jp9093172.

[4]   D.R. Pereira, C. Díaz-Guerra, M. Peres, S. Magalhães, J.G. Correia, J.G. Marques, A.G. Silva, E. Alves, K. Lorenz, Engineering strain and conductivity of MoO_3 by ion implantation, Acta Mater. 169 (2019) 15–27. doi:10.1016/j.actamat.2019.02.029.

[5]   A. Debelle, A. Declémy, L. Vincent, F. Garrido, L. Thomé, XRD contribution to the study of Cs-implanted cubic zirconia, J. Nucl. Mater. 396 (2010) 240–244. doi:10.1016/j.jnucmat.2009.11.016.

[6]   A. Boulle, A. Debelle, J.B. Wallace, L.B. Bayu Aji, S.O. Kucheyev, The amorphization of 3C-SiC irradiated at moderately elevated temperatures as revealed by X-ray diffraction, Acta Mater. 140 (2017) 250–257. doi:10.1016/j.actamat.2017.08.030.

[7]   P. Jozwik, S. Magalhães, R. Ratajczak, C. Mieszczynski, M. Sequeira, A. Turos, R. Böttger, R. Heller, K. Lorenz, E. Alves, RBS/C, XRR, and XRD Studies of Damage Buildup in Er-Implanted ZnO, Phys. Status Solidi. 256 (2019) 1800364. doi:10.1002/pssb.201800364.

[8]   D.N. Faye, E. Wendler, M. Felizardo, S. Magalhães, E. Alves, F. Brunner, M. Weyers, K. Lorenz, Mechanisms of Implantation Damage Formation in $Al_xGa_{1-x}N$ Compounds, J. Phys. Chem. C. 120 (2016) 7277–7283. doi:10.1021/acs.jpcc.6b00133.

[9]   B. Lacroix, S. Leclerc, A. Declémy, K. Lorenz, E. Alves, P. Ruterana, Mechanisms of damage formation in Eu-implanted GaN probed by X-ray diffraction, Europhys. Lett. 96 (2011) 46002. doi:10.1209/0295-5075/96/46002.

[10]   A. Turos, P. Jóźwik, M. Wójcik, J. Gaca, R. Ratajczak, A. Stonert, Mechanism of damage buildup in ion bombarded ZnO, Acta Mater. 134 (2017) 249–256. doi:10.1016/j.actamat.2017.06.005.

[11] A. Debelle, J.-P. Crocombette, A. Boulle, A. Chartier, T. Jourdan, S. Pellegrino, D. Bachiller-Perea, D. Carpentier, J. Channagiri, T.-H. Nguyen, F. Garrido, L. Thomé, Lattice strain in irradiated materials unveils a prevalent defect evolution mechanism, Phys. Rev. Mater. 2 (2018) 013604. doi:10.1103/PhysRevMaterials.2.013604.

[12] J. Channagiri, A. Boulle, A. Debelle, Determination of strain and damage profiles in irradiated materials: Application to cubic zirconia irradiated at high temperature, Nucl. Instruments Methods Phys. Res. Sect. B Beam Interact. with Mater. Atoms. 327 (2014) 9–14. doi:10.1016/j.nimb.2013.10.086.

[13] N. Mejai, A. Debelle, L. Thomé, G. Sattonnay, D. Gosset, A. Boulle, R. Dargis, A. Clark, L. Thom, Depth-dependent phase change in Gd_2O_3 epitaxial layers under ion irradiation, Appl. Phys. Lett. 107 (2015) 131903. doi:10.1116/1.4882173.

[14] A. Debelle, J. Channagiri, L. Thomé, B. Décamps, A. Boulle, S. Moll, F. Garrido, M. Behar, J. Jagielski, Comprehensive study of the effect of the irradiation temperature on the behavior of cubic zirconia, J. Appl. Phys. 115 (2014) 183504. doi:10.1063/1.4874795.

[15] S. Magalhães, M. Fialho, M. Peres, K. Lorenz, E. Alves, Quantitative x-ray diffraction analysis of bimodal damage distributions in Tm implanted $Al_{0.15}Ga_{0.85}N$, J. Phys. D. Appl. Phys. 49 (2016) 135308.

[16] M. Vila, C. Díaz-Guerra, D. Jerez, K. Lorenz, J. Piqueras, E. Alves, Intense luminescence emission from rare-earth-doped MoO_3 nanoplates and lamellar crystals for optoelectronic, J. Phys. D. Appl. Phys. 47 (2014) 355105. doi:10.1088/0022-3727/47/35/355105.

[17] D.R. Pereira, M. Peres, L.C. Alves, J.G. Correia, C. Díaz-Guerra, A.G. Silva, E. Alves, K. Lorenz, Electrical characterization of molybdenum oxide lamellar crystals irradiated with UV light and proton beams, Surf. Coatings Technol. 355 (2018) 50–54. doi:10.1016/j.surfcoat.2018.01.034.

[18] J.F. Ziegler, J.P. Biersack, U. Littmark, The Stopping and Range of Ions in Solids, Pergamon, New York, 1985. http://www.srim.org/.

[19] M. Souilah, A. Boulle, A. Debelle, RaDMaX: A graphical program for the determination of strain and damage profiles in irradiated crystals, J. Appl. Crystallogr. 49 (2016) 311–316. doi:10.1107/S1600576715021019.

[20] A. Boulle, A. Chartier, J.P. Crocombette, T. Jourdan, S. Pellegrino, A. Debelle, Strain and damage build-up in irradiated crystals: Coupling X-ray diffraction with numerical simulations, Nucl. Instruments Methods Phys. Res. Sect. B Beam Interact. with Mater. Atoms. 458 (2018) 143–150. doi:10.1016/j.nimb.2018.11.048.

[21]   V.S. Speriosu, Kinematical x-ray diffraction in nonuniform crystalline films: Strain and damage distributions in ion-implanted garnets, J. Appl. Phys. 52 (1981) 6094. doi:10.1063/1.328549.

[22]   A. Boulle, R. Guinebretière, A. Dauger, Phenomenological analysis of heterogeneous strain fields in epitaxial thin films using x-ray scattering, J. Phys. D. Appl. Phys. 38 (2005) 3907–3920. doi:10.1088/0022-3727/38/21/012.

[23]   S. Creutzburg, E. Schmidt, P. Kutza, R. Loetzsch, I. Uschmann, A. Undisz, M. Rettenmayr, F. Gala, G. Zollo, A. Boulle, A. Debelle, E. Wendler, Defects and mechanical properties in weakly damaged Si ion implanted GaAs, Phys. Rev. B. 99 (2019) 245205. doi:10.1103/PhysRevB.99.245205.

[24]   A. Boulle, A. Debelle, Strain-profile determination in ion-implanted single crystals using generalized simulated annealing, Appl. Crystallogr. 43 (2010) 1046–1052. doi:10.1107/S0021889810030281.

[25]   S. Milita, M. Servidori, X-ray Rocking-Curve Analysis of Crystals with Buried Amorphous Layers. Case of Ion-Implanted Silicon, J. Appl. Cryst. 28 (1995) 666–672.

[26]   J.G.E. Klappe, P.F. Fewster, Fitting of Rocking Curves from Ion-Implanted Semiconductors, J. Appl. Crystallogr. 27 (1994) 103–110. doi:10.1107/S0021889893007484.